Chinese Chemical Letters 32 (2021) 3431–3434

Contents lists available at ScienceDirect

Chinese Chemical Letters

journal homepage: www.elsevier.com/locate/cclet

Communication

Enhanced photocatalytic degradation of sulfamethoxazole by stable hierarchical Fe_2O_3/Co_3O_4 heterojunction on nickel foam

Jinli Qiu, Cailiang Yue, Wenting Zheng, Fuqiang Liu*, Junjie Zhu

School of the Environment & School of Chemistry and Chemical Engineering, Nanjing University, Nanjing 210023, China

ARTICLE INFO

Article history:
Received 20 February 2021
Revised 6 April 2021
Accepted 14 May 2021
Available online 19 May 2021

Keywords:
Photocatalysis
Sulfamethoxazole
Ni foam
Fe_2O_3
CO_3O_4

ABSTRACT

A facile approach was successfully employed to prepare Fe_2O_3/Co_3O_4 nanosheet arrays on nickel foams (Fe_2O_3/Co_3O_4@NF), which owned such advantages as narrow band gap energies and high separation rate of photoexcited electron-hole pairs. The combination of Fe_2O_3 and Co_3O_4 dramatically enhanced the photocatalytic activity towards sulfamethoxazole (SMZ) degradation, with the highest catalytic efficiency of $k = 0.0538$ min^{-1}, which was much higher than that of Fe_2O_3@NF (0.0098 min^{-1}) and Co_3O_4@NF (0.0094 min^{-1}). The introduction of Ni foam could not only act as the support to anchor photocatalyst, but also work as the electron mediator to promote the transition of electron-hole pairs. Reactive species trapping experiments combined with electron paramagnetic resonance analysis confirmed $^{\bullet}O_2^-$ was primarily responsible for SMZ degradation. Furthermore, Fe_2O_3/Co_3O_4@NF was effective and almost unaffected by inorganic cations and anions in aqueous solution. This study could provide a facile and promising path for the construction of self-supported metal oxide-based heterojunction with high efficiency and strong stability.

Antibiotics pollution has attracted extensive attention because of its great threat to ecosystem security and human health [1]. Traditional activated sludge process exhibited rather low removal efficiency and long processing cycle, which limited its application [2]. Recently, advanced oxidation processes (AOPs) including persulfate (PS) activation, photocatalysis and Fenton, have been proved to be promising methods for the removal of antibiotics [3–5]. Compared with PS activation and Fenton, heterogeneous photocatalysis technology has been a research hotspot due to the low energy consumption, mild reaction condition and free secondary pollution [6–10]. However, the fairly low photocatalytic efficiency and visible light utilization rate limited its further applications. Besides, nanoscale photocatalysts were facile to reunite and difficult to recycle, which was another problem for its development. Therefore, constructing photocatalysts with high photocatalytic efficiency and easy recycling ability is of great challenge.

Fe_2O_3 is an n-type semiconductor with the band gap of ~2.0 eV, which has been widely used in photocatalysis and photo-Fenton processes due to its natural abundance, non-toxicity and excellent visible light adsorption [11,12]. Nevertheless, low surface area and high recombination rate of photo-generated carrier are the bottlenecks of Fe_2O_3 [13]. Coupling Fe_2O_3 with other semiconductor photocatalysts to construct heterojunctions, such as TiO_2, MIL-53(Fe) and Bi_2WO_6, is an efficient way to promote the separation of electron-hole pairs [14–16]. Compared with traditional type-II heterostructure, the Z-scheme heterostructure has been a hotpot because of the high separation efficiency of photo-generated carrier and the unchanged photocatalytic abilities [17,18]. Therefore, several Z-scheme photocatalysts based on Fe_2O_3 have been developed to obtain superior photocatalytic activities, such as Fe_2O_3/g-C_3N_4, Fe_2O_3/MIL-101(Cr) and Fe_2O_3/MoS_2 [11,19,20]. Co_3O_4 is a widely studied p-type semiconductor in CO_2 reduction and water oxidation, as the suitable energy band structure [21,22]. Considering the different energy band structures between Fe_2O_3 and Co_3O_4, it is rational to design a Z-scheme heterojunction of Fe_2O_3/Co_3O_4.

To improve the stability and recycling performance of photocatalysts, common method is loading the photocatalysts onto suitable support, including hydrogel, aerogel, carbon materials, SiO_2, Al_2O_3 [23–27]. Generally, the photocatalytic efficiency sharply decreased due to the weak electrical conductivity and obstructive light adsorption of substrate. Recently, the growth of photocatalysts on the electrically conductive substrates with open framework structures, such as Ni foam, has been proved as an effective approach for preparing efficient self-supported photocatalysts [28–30].

Herein, in this study, Fe_2O_3 and Co_3O_4 nanosheet arrays were incorporated into a Z-scheme heterojunction and loaded on the Ni foam through facile method. The prepared Fe_2O_3/Co_3O_4@NF was

* Corresponding author.
E-mail address: lfq@nju.edu.cn (F. Liu).

https://doi.org/10.1016/j.cclet.2021.05.022
1001-8417/

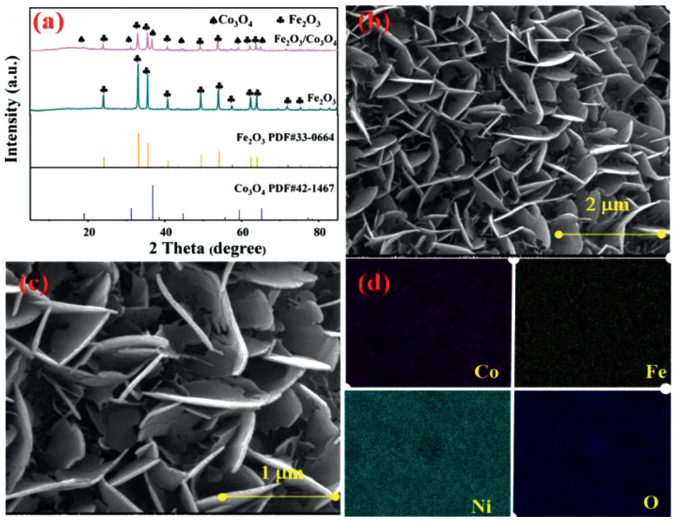

Fig. 1. XRD patterns of as-prepared samples (a), SEM images with different scales: 2 μm (b) and 1 μm (c) and the corresponding element mappings for Co, Fe, Ni and O of Fe_2O_3/Co_3O_4@NF (d).

further employed for the degradation of sulfamethoxazole (SMZ) under simulated solar light irradiation. Fe_2O_3/Co_3O_4@NF with different preparation parameters were also fabricated for comparison. Detailed synthesis procedure, characterization and photocatalytic performance evaluation were given in the Supporting information (SI).

X-ray Electron Diffraction (XRD) is a powerful approach to determine the crystal structure of the materials. The XRD patterns of Fe_2O_3 and Fe_2O_3/Co_3O_4 were shown in Fig. 1a. Two phases of Fe_2O_3 and Co_3O_4 could be observed from the XRD spectrum. The peaks at 2θ = 24.1°, 33.2°, 35.6°, 40.8°, 49.5° and 54.1° were indexed to the (012), (104), (110), (113), (024) and (116) planes of hexagonal Fe_2O_3 (JCPDS No. 333-0664), respectively [31]. The diffraction peaks of cubic Co_3O_4 (JCPDS No. 42-1467) at 2θ = 19.0°, 31.3°, 36.9°, 44.8°, 59.4° and 65.2° were attributed to the (111), (220), (311), (400), (511) and (440) planes [32].

The surface morphology of Fe_2O_3/Co_3O_4@NF was demonstrated in Figs. 1b and c *via* scanning electron microscope (SEM). Fe_2O_3/Co_3O_4@NF exhibited a hierarchical structure with Fe_2O_3/Co_3O_4 nanosheet arrays interconnected with each other, forming a highly open three-dimensional network. As shown in Fig. 1d, energy dispersive X-ray spectroscopy (EDS) mapping revealed uniform spatial distribution of Fe, Co, Ni and O elements in Fe_2O_3/Co_3O_4@NF.

The surface chemical compositions of Fe_2O_3/Co_3O_4@NF were obtained by X-ray photoelectron spectroscopy (XPS). The survey spectrum confirmed the existence of O, Fe, Ni and Co elements in the Fe_2O_3/Co_3O_4@NF (Fig. S1 in Supporting information), which was in well agreement with the elemental mapping results. As depicted in Fig. 2a, the peaks at the binding energy of 710.0 eV and 725.5 eV were ascribed to Fe $2p_{3/2}$ and Fe $2p_{1/2}$ of Fe 2p, respectively. As revealed in Fig. 2b, the high-resolution Co 2p spectrum was obtained by fitting into six components, including four peaks (776.2 eV, 780.8 eV, 796.5 eV, 802.1 eV) of Co 2p and two shakeup satellites (785.8 eV and 806.7 eV), which matched well with those characteristic peaks of Co_3O_4 [33]. As presented in Fig. 2c, the peaks of O 1s located at 530.6 eV, 531.4 eV and 532.3 eV were corresponded to lattice oxygen, hydroxyl oxygen and adsorbed oxygen in Fe_2O_3/Co_3O_4@NF, respectively. All of these indicated the successful fabrication of Fe_2O_3/Co_3O_4@NF.

The transient photocurrent and EIS (Electrochemical Impedance Spectroscopy) were employed to analyze the photogenerated carrier separation efficiency of fabricated samples. It can be seen that photocurrent density was obviously enhanced for Fe_2O_3/Co_3O_4 (Fig. 3a). Besides, the arc radius of Fe_2O_3/Co_3O_4 was smaller than that of Fe_2O_3 and Co_3O_4, indicating its small charge transfer resistance and the fast electron mobility (Fig. 3b). The fabrication parameters of materials seriously affect their photocatalytic degradation performance. Therefore, the photocatalytic activities of Fe_2O_3/Co_3O_4@NF with different fabrication parameters were investigated through degradation of SMZ in aqueous solution under simulated solar light irradiation. As presented in Fig. 3c, the Fe_2O_3/Co_3O_4@NF-2 obtained the optimal degradation performance, and the corresponding k value is 0.0538 min^{-1}, which is much higher than those for other samples. Additionally, the total organic carbon (TOC) removal efficiency for SMZ on Fe_2O_3/Co_3O_4@NF-2 was 31.5%. The effects of solution pH, inorganic anions and cations on SMZ removal were carried out and the results were presented in Fig. S2 (Supporting information). Reusability and stability of photocatalysts have remarkable influence on their practical applications. Therefore, five consecutive cycles for SMZ degradation experiment on the fabricated photocatalyst were performed. As shown in Fig. 3d, there was no obvious decay on SMZ degradation after five cycles, which indicated the excellent reusability and stability of Fe_2O_3/Co_3O_4@NF. River water and tap water was sampled and employed for the preparation of the spiked samples. As depicted in Fig. S3 (Supporting information), the degradation efficiency for SMZ by Fe_2O_3/Co_3O_4@NF in spiked water was 68.3% and 83.5%, respectively, indicating its excellent potential for practical applications.

To further explore the degradation mechanism of SMZ, active species trapping experiment was carried out to verify the primary free radicals in the photocatalytic process. According to the previous published literatures, AO (ammonium oxalate), NBT (nitroblue tetrazolium), FFA (furfuryl alcohol) and IPA (isopropanol) were employed as the scavengers of hole, $^{\bullet}O_2^-$, $^1O_2$ and $^{\bullet}OH$, respectively. As depicted in Fig. 4a, the degradation efficiency of SMZ decreased distinctly from 100% to 29.35% with the addition of NBT, indicating the important role of $^{\bullet}O_2^-$in the photo-degradation of SMZ. Meanwhile, the addition of IPA and FFA also has negative effect on the removal efficiency of SMZ. The above results of trapping experiment were consistent with the EPR characterization (Fig. S4 in Supporting information).

The degradation products of SMZ were analyzed by electrospray mass spectrometry (ESI-MS), and the possible degradation pathway of SMZ was presented in Fig. S5 (Supporting information). The cleavage of either N-S bond or N-C bond on SMZ is to yield 5-Methylisoxazol-3-amine (M_w = 98), benzene sulfonamide (M_w = 157) and 4-aminobenzenesulfonamide (M_w = 172). Besides, the product with a molecular weight of 213 is due to the destruction of isoxazole ring on SMZ. After that, the above intermediate products were transferred into acids with small molecular weight such as maleic acid (M_w = 116) and pyruvic acid (M_w = 88). Finally, these small acids are mineralized.

As depicted in Figs. 4b and c, the band gap for Fe_2O_3 and Co_3O_4 was 2.24 eV and 1.70 eV, respectively [34,35]. Meanwhile, the potential of conduction band for Fe_2O_3 and valence band for Co_3O_4 was –0.21 eV and 1.0 eV, respectively (Fig. S6 in Supporting information). Herein, the potential of valence band for Fe_2O_3 and conduction band for Co_3O_4 was calculated to be 2.03 eV and –0.70 eV, respectively. According to the band gap structures of Fe_2O_3 and Co_3O_4, the enhanced photocatalytic mechanism was proposed in Fig. 4d. Because of the strong built-in electric field resulted from the different energy band structures, fast photo-generated carriers separation occurred in the interface of Fe_2O_3/Co_3O_4 heterojunction. Ni foam not only acted as support to enhance the stability of Fe_2O_3/Co_3O_4 heterojunction, but also worked as an electron medi-

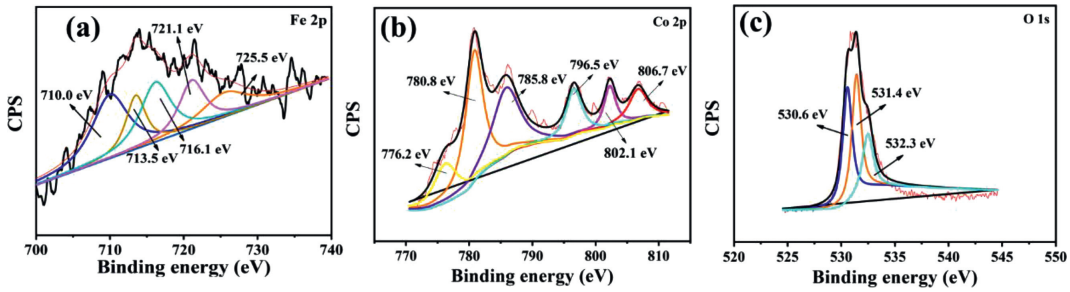

Fig. 2. XPS spectra of the Fe_2O_3/Co_3O_4@NF: high-resolution scan of (a) Fe 2p, (b) Co 2p and (c) O 1s.

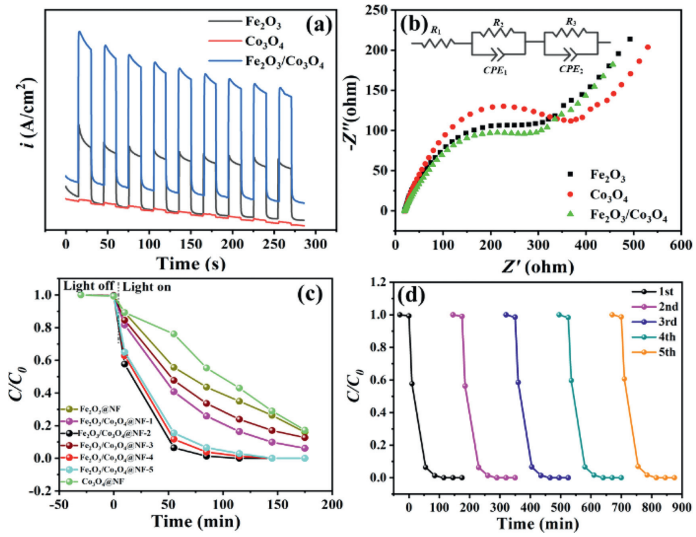

Fig. 3. (a) Transient photocurrent spectra and (b) EIS spectra of the as-prepared samples. (c) Photocatalytic performance for SMZ degradation on different photocatalysts and (d) recycling experiment of Fe_2O_3/Co_3O_4@NF towards SMZ degradation under simulated solar light irradiation.

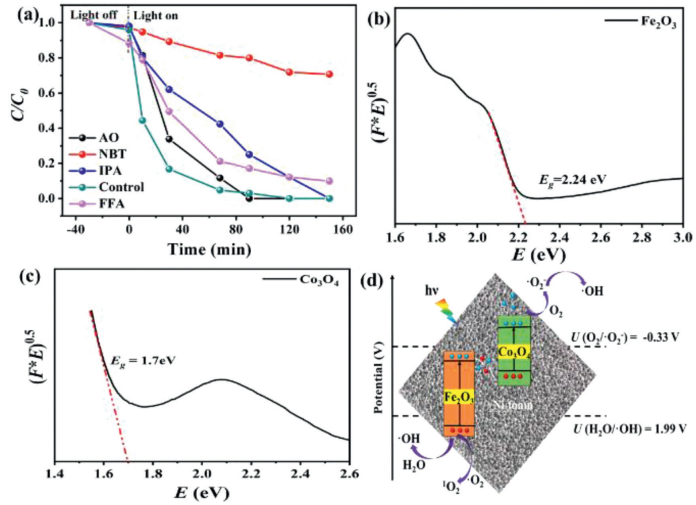

Fig. 4. (a) Active species trapping experiment for SMZ degradation on the prepared Fe_2O_3/Co_3O_4@NF. Band gap of Fe_2O_3 (b) and Co_3O_4 (c). (d) Degradation mechanism of Fe_2O_3/Co_3O_4@NF towards SMZ under simulated solar light irradiation.

ator to boost photo-generated charrier separation as the good electrical conductivity.

In summary, a Z-scheme Fe_2O_3/Co_3O_4 heterojunction was fabricated on Ni foam by a facile method. The highest rate constant k (0.0538 min^{-1}) was of Fe_2O_3/Co_3O_4@NF-2, which was much higher than that of Fe_2O_3@NF (0.0098 min^{-1}) and Co_3O_4@NF (0.0094 min^{-1}). The unique Z-scheme heterojunction structure not only enhanced the absorption of visible light, but also boosted the transfer of photo-excited electrons and holes due to the well staggered energy band structures between Fe_2O_3 and Co_3O_4. Ni foam served as efficient electron mediator and supporter to enhance the activities and stability of Fe_2O_3/Co_3O_4 heterojunction. This work may provide a reference of utilizing Ni foam as a novel support and constructing Z-scheme heterojunction to obtain semiconductor photocatalysts with remarkable efficiency and strong stability.

Declaration of competing interest

The authors declare that they have no known competing financial interests or personal relationships that could have appeared to influence the work reported in this paper.

Acknowledgments

The authors gratefully acknowledge the support of Postdoctoral Science Foundation of Jiangsu Province (No. 2020Z299) and China Postdoctoral Science Foundation (No. 2020M671443).

Supplementary materials

Supplementary material associated with this article can be found, in the online version, at doi:10.1016/j.cclet.2021.05.022.

References

[1] A.Z. Baygi, M. Harb, P. Wang, et al., Environ. Sci. Technol. 53 (2019) 3599–3609.
[2] A.S. Oberoi, Y. Jia, H. Zhang, et al., Environ. Sci. Technol. 53 (2019) 7234–7264.
[3] J. Lim, Y. Yang, M.R. Hoffmann, Environ. Sci. Technol. 53 (2019) 6972–6980.
[4] T. Li, C. Wang, T. Wang, et al., Appl. Catal. B: Environ. 268 (2020) 118442.
[5] P. Zhou, J. Zhang, Z. Xiong, et al., Appl. Catal. B: Environ. 265 (2020) 118264.
[6] A.G. Sanchez, M.G. Mendoza, M. Barawi, et al., J. Am. Chem. Soc. 142 (2020) 318–326.
[7] X. Xiao, C. Zheng, M. Lu, et al., Appl. Catal. B: Environ. 228 (2018) 142–151.
[8] X. Feng, Y. Pi, Y. Song, et al., J. Am. Chem. Soc. 142 (2020) 690–695.
[9] D.Y. Ni, Y.Y. Zhang, Y.F. Shen, et al., Chin. Chem. Lett. 31 (2020) 115–118.
[10] T.X. Xu, J.P. Wang, Y. Cong, et al., Chin. Chem. Lett. 31 (2020) 1022–1025.
[11] M. Guo, Z. Xing, T. Zhao, et al., Appl. Catal. B: Environ. 272 (2020) 118978.
[12] Y.L. Wang, Y.H. Li, X.L. Wang, et al., Appl. Catal. B: Environ. 206 (2017) 216–220.
[13] J. Wang, C. Qin, H. Wang, et al., Appl. Catal. B: Environ. 221 (2018) 459–466.
[14] L. Ren, W. Zhou, B. Sun, et al., Appl. Catal. B: Environ. 240 (2019) 319–328.
[15] Q. Wu, Y. Liu, H. Jing, et al., Chem. Eng. J. 390 (2020) 124615.
[16] S. Adhikari, S. Selvaraj, D.H. Kim, Appl. Catal. B: Environ. 244 (2019) 11–24.
[17] P. Zhou, J. Yu, M. Jaroniec, Adv. Mater. 26 (2014) 4920–4935.
[18] M. Ding, J.J. Zhou, H.C. Yang, et al., Chin. Chem. Lett. 31 (2020) 71–76.
[19] Y. Geng, D. Chen, N. Li, et al., Appl. Catal. B: Environ. 280 (2021) 119409.
[20] Q. Huo, X. Qi, J. Li, et al., Appl. Catal. B: Environ. 255 (2019) 117751.
[21] L. Wang, J. Wan, Y. Zhao, et al., J. Am. Chem. Soc. 141 (2019) 2238–2241.
[22] H. Zhang, W. Tian, L. Zhou, et al., Appl. Catal. B: Environ. 223 (2018) 2–9.
[23] Y. Hu, Z. Li, J. Yang, et al., Chem. Eng. J. 360 (2019) 200–211.
[24] Z. Cai, X. Hao, X. Sun, et al., Water Res. 162 (2019) 369–382.
[25] S. Shanavas, S.M. Roopan, A. Priyadharsan, et al., Appl. Catal. B: Environ. 255 (2019) 117758.

[26] Y. Tian, W. Li, C. Zhao, et al., Appl. Catal. B: Environ. 213 (2017) 136–146.
[27] Q. Nie, Y. Xie, J. Ma, et al., J. Clean. Prod. 242 (2020) 118532.
[28] Q. Wu, A. Dong, C. Yang, et al., Chem. Eng. J. 413 (2020) 127482.
[29] W. Fei, J. Gao, N. Li, et al., J. Hazard. Mater. 402 (2021) 123515.
[30] Q. Zhao, Y. Zheng, C. Song, et al., Appl. Catal. B: Environ. 265 (2020) 118552.
[31] Y. Jin, L. Dang, H. Zhang, et al., Chem. Eng. J. 326 (2017) 292–297.
[32] A. Al Nafiey, A. Addad, B. Sieber, et al., Chem. Eng. J. 322 (2017) 375–384.
[33] C. Zhu, M. Zhu, Y. Sun, et al., ACS Appl. Energ. Mater. 2 (2019) 8737–8746.
[34] D. Zhang, B. Mao, D. Li, et al., Chem. Eng. J. 417 (2020) 128275.
[35] C.H. Shen, X.J. Wen, Z.H. Fei, et al., Chem. Eng. J. 391 (2020) 123612.